Photoionization efficiency spectrum and ionization energy of HSO studied by discharge flow-photoionization mass spectrometry

Bing-Ming Cheng[a)]
Synchrotron Radiation Research Center, No. 1, R&D Road VI, Hsinchu Science-Based Industrial Park, Hsinchu 30077, Taiwan, Republic of China

Jürg Eberhard, Wei-Chen Chen, and Chin-hui Yu
Department of Chemistry, National Tsing Hua University, No. 101, Sec. 2, Kuang Fu Road, Hsinchu 30043, Taiwan, Republic of China

(Received 22 November 1996; accepted 14 March 1997)

The photoionization efficiency (PIE) spectrum of HSO was measured in the spectral range (107–130) nm by means of a discharge flow and a photoionization mass spectrometer coupled to a synchrotron as the radiation source. HSO radicals were generated by reacting O atoms with various organothiol compounds, C_2H_5SH, 2-C_3H_7SH, or HSC_2H_4SH, in the flow tube. The ionization energy of HSO was determined for the first time and found to be (9.918 ± 0.016) eV. GAUSSIAN-2 calculations predict 9.897 eV for ionization to HSO^+, the singlet ground state of the molecular ion, in satisfactory agreement with the experimental result. The onset to triplet HSO^+ may occur at (11.15 ± 0.04) eV. A vibrational frequency of HSO^+ of (1150 ± 160) cm^{-1} was derived from the separation of steps in the PIE spectrum. The heat of formation of HSO^+ was also derived and calculated to be $\Delta_f H^\circ_{298}(HSO^+)=(228\pm5)$ kcal mol^{-1}. © *1997 American Institute of Physics.* [S0021-9606(97)03423-5]

I. INTRODUCTION

Hydrogen sulfide is a major reduced sulfur compound in the atmosphere.[1] Oxidation of such sulfur compounds leads to acidic precipitation. The atmospheric degradation of H_2S is initiated by reaction with hydroxyl radicals,[2–4] which can form HS radicals,

$$OH+H_2S\rightarrow HS+H_2O. \quad (1)$$

Further oxidation of HS radicals with O_3 (Refs. 5–8) or NO_2 (Refs. 9 and 10) in the atmosphere can generate HSO radicals,

$$HS+O_3\rightarrow HSO+O_2, \quad (2)$$

$$HS+NO_2\rightarrow HSO+NO. \quad (3)$$

Reaction of O atoms with RSH (in which R=H, CH_3, or C_2H_5)[11,12] also produces HSO,

$$O+RSH\rightarrow HSO+R. \quad (4)$$

Subsequent oxidation of HSO leads to formation of SO_2 and eventually to H_2SO_4. Thus HSO is a key intermediate in the oxidation of reduced sulfur compounds in the atmosphere.

HSO is characterized spectroscopically by laser-induced fluorescence,[13–17] laser-magnetic resonance,[18,19] microwave spectra,[20] intracavity laser absorption,[21–23] and chemiluminescence,[7] but no photoionization spectrum is reported. In kinetic experiments photoionization mass spectrometry was employed to detect HSO. It is important to measure photoionization spectra of HSO so that an optimal wavelength for ionization of HSO in kinetic studies can be established.

In the present work we measure photoionization efficiency spectra (PIE) of HSO by using a discharge flow-photoionization mass spectrometric apparatus (DF-PIMS) coupled to a synchrotron as the ionizing source. HSO radicals are generated from the reactions of oxygen atoms with various organothiol compounds in the flow tube. The ionization energy (IE) of HSO is determined from the PIE spectrum. In order to assess the reliability of the experimental results, we employ *ab initio* calculations on HSO and HSO^+ using the GAUSSIAN-2 (G2) theoretical procedure. Predictions obtained in these calculations are compared to the experimental results.

II. EXPERIMENTAL SECTION AND THEORETICAL METHODS

A. Experiment

The discharge flow-photoionization mass spectrometer coupled to a synchrotron as an ionization source is described in detail elsewhere;[24] only matters pertinent to this experiment are explained here. A 30-cm-long Pyrex™ flow tube with 25 mm i.d. was used. To minimize possible surface reactions, a Teflon™ tube (i.d. 22 mm) was inserted into the flow tube.

HSO radicals were generated via the reaction of atomic oxygen with organothiol compounds. O atoms were produced in a sidearm of the flow tube by flowing O_2/He mixtures through a microwave discharge. The organothiol compounds were added to the reaction region of the flow tube in a stream of He through a movable injector (o.d. 8 mm). The $O+CH_3SH$ reaction is unsuited for the generation of HSO radicals because the product ion HSO^+ ($m/z=49$) is difficult to resolve from the parent ion CH_3SH^+ ($m/z=48$). Therefore HSO radicals were generated from the reactions of

[a)]Author to whom all correspondence should be addressed.

O atoms with C_2H_5SH, 2-C_2H_7SH, or HSC_2H_4SH. The rate coefficients for the $O+CH_3SH$ and $O+C_2H_5SH$ reactions at 298 K are 2.0 and 3.0×10^{-12} cm^3 $molecule^{-1}$ s^{-1}, respectively.[25] Although no rate coefficients for the reactions of O atoms with other organothiol compounds are reported, we believe that the $O+2$-C_3H_7SH and $O+HSC_2H_4SH$ reactions are also fast and that these reactions are also suitable to produce HSO radicals. Attempts were also made to generate HSO radicals through reaction (3). HS radicals were generated from the $Cl+H_2S$ reaction. We were unable to produce sufficient amounts of HSO radicals, most probably because the radicals were efficiently lost through the fast reaction with NO_2.

The pressure in the flow tube was regulated with a rotary pump and maintained at (0.5–1.5) Torr. The effluents in the flow tube were sampled into a second chamber through a Teflon diaphragm with a hole of 2 mm in diameter. A turbomolecular pump ($1000\,\ell\,s^{-1}$) was employed to maintain pressures below 2×10^{-4} Torr in the second chamber. The effluents were subsequently sampled through a Teflon skimmer with an orifice of 3 mm in diameter into the ionization region of the mass spectrometer. Another turbomolecular pump ($1000\,\ell\,s^{-1}$) served to maintain pressures below 8×10^{-6} Torr in this ionization chamber. The ions were selected with a quadrupole mass filter aligned in the axial direction and detected with a channeltron.

The radiation for photoionization was conducted through a 1 m Seya–Namioka monochromator from the 1.3 GeV storage ring of the Synchrotron Radiation Research Center in Taiwan.[26] The photoionization spectra were normalized for intensity variations in the ionizing source by procedures described before.[24] The intensity of the zero-order light was recorded to calibrate the monochromator at the beginning and to verify the calibration at the end of each injection of the storage ring.[24,27] A LiF window (2 mm thick) was placed between the ionizing chamber and the exit port of the monochromator to suppress radiation of second and higher orders from the grating.

Typical flow conditions were as follows: total flow rate: $F_T=(5.5–7.5)$ STP cm^3 s^{-1}; flow rate of O_2: $F_{O_2}=0.02$ STP cm^3 s^{-1}; vapor flow rate of organothiol compound (RSH): $F_{RSH}=(0.1–0.2)$ STP cm^3 s^{-1}; flow rate of He to carry O_2: $F_{He/O_2}=2.0$ STP cm^3 s^{-1}; flow rate of He to carry the vapor of RSH: $F_{He/RSH}=(0.2–2.0)$ STP cm^3 s^{-1}.

Laboratory gases (Matheson) of He (99.9995%) and O_2 (99.997%) were directly used without further purification. Ethanethiol (>99%), 2-propanethiol (>98%), and 1,2-ethanedithiol (>99%) were purchased from Merck, and the first fifth of the liquid samples were pumped away before use.

B. Computational methods

The *ab initio* G2 method[28] was employed to calculate the ionization energy of HSO. The energies E_{G2} of HSO and HSO^+ were computed at the optimized geometry, obtained from a MP2 perturbation calculation with a 6-31(d) basis set, and all electrons were included [MP2(full)/6-31(d)].

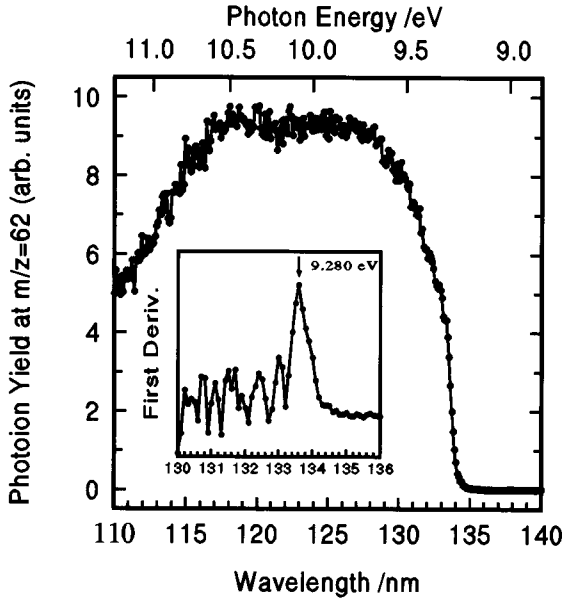

FIG. 1. Photoionization efficiency spectrum of C_2H_5SH ($m/z=62$) at a nominal resolution of 0.1 nm and with 0.1 nm steps. The concentration of C_2H_5SH in He was 2.4%. The first derivative of the PIE spectrum near the onset region is shown in the inset. The arrow indicates the ionization energy of C_2H_5SH.

The zero-point energies were evaluated with harmonic frequencies from HF/6-31(d) scaled by 0.8929. To compute the vertical IE, the G2 level energy of HSO^+ $E_{G2'}$ was deduced from single point calculations with geometry optimized at the MP2(full)/6-31(d) level of HSO, which is the most stable structure of the neutral molecule. The single point calculations required for the ion included QCISD(T,E4T)/6-311(d,p), MP4/6-311+(d,p), MP4/6-311+($2df,p$), and MP2/6-311+($3df,2p$). Possible vibrational excitation of the ion associated with the vertical transition was not treated explicitly and the zero-point energy of the ion was used as an approximation. Program suite GAUSSIAN 94[29] was used to perform the G2 and single point calculations for $E_{G2'}$(HSO) in order to obtain IE and $IE_{vertical}$ of HSO.

III. RESULTS AND DISCUSSION

A. PIE spectrum and IE of C_2H_5SH

Photoionization efficiency spectra of various reactants were measured first to establish the performance of the PIMS system. Figure 1 shows the PIE spectrum of C_2H_5SH over the wavelength range $\lambda=(110–140)$ nm. The spectrum was obtained by monitoring the ion counts at $m/z=62$ that are normalized with respect to relative intensities of the ionizing source at varied wavelengths. This spectrum was scanned in 0.1 nm steps at a slit width of 0.05 mm, corresponding to a nominal resolution of about 0.1 nm.

The spectrum displays an abrupt onset, characteristic for direct ionization through the $0\rightarrow0$ transition and thus indicating similar geometries of the electronic ground states of both the ion and the neutral molecule. The first derivative of the PIE spectrum [d(PIE)/$d\lambda$], near the threshold region

TABLE I. Ionization energies (in eV) measured in this work.

Species	This work	Previous results	Reference
C_2H_5SH	9.280±0.007[a]	9.285±0.005	30
2-C_3H_7SH	9.143±0.007[a]	9.14	31
HSC_2H_4SH	9.280±0.014[a]		
HSO	9.918±0.016[b]		

[a]Uncertainty derived from instrumental resolution.
[b]Uncertainty limits represent 2σ (see Table II).

(130–136) nm is plotted in the inset of Fig. 1, which contains one relatively sharp feature. The ionization threshold was determined from the maximum of the first derivative curve, which appears at (133.6±0.1) nm, as indicated by the arrow in Fig. 1. This threshold corresponds to an ionization energy of (9.280±0.007) eV, in excellent agreement with the value (9.285±0.005) eV measured with the photoionization method.[30] Hence, it is demonstrated that the DF-PIMS system operates properly and the wavelength calibration, established by adjusting to the maximum intensity of the zero-order light, is reliable. The results are summarized in Table I.

B. PIE spectrum and IE of 2-C_3H_7SH

The PIE spectrum of 2-C_3H_7SH was measured similarly as for C_2H_5SH and is shown in Fig. 2. As photoionization of organothiol compounds involves the removal of an essentially nonbonding electron from a $3p$ lone pair localized on a sulfur atom, the PIE features near the threshold region for these compounds are expected to be sharp.[31] Thus as the photon energy is increased, the PIE signals for organothiol compounds are found to increase steeply from the threshold.

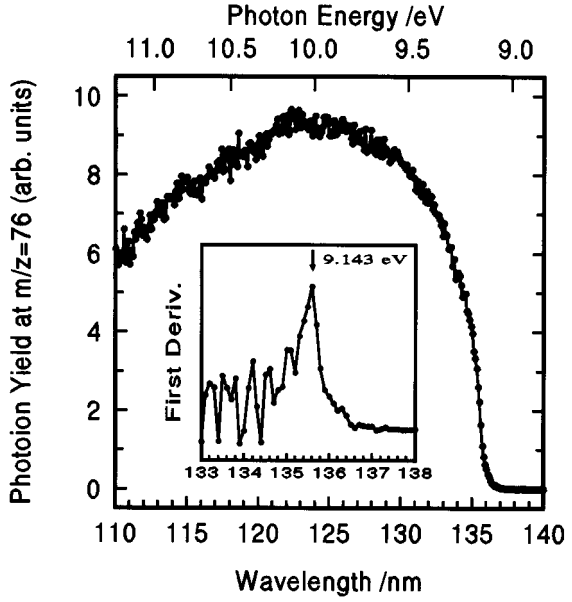

FIG. 2. Photoionization efficiency spectrum of 2-C_3H_7SH ($m/z=76$) at a nominal resolution of 0.1 nm and with 0.1 nm steps. The concentration of 2-C_3H_7SH in He was 1.5%. The first derivative of the PIE spectrum near the onset region is shown in the inset. The arrow indicates the ionization energy of 2-C_3H_7SH.

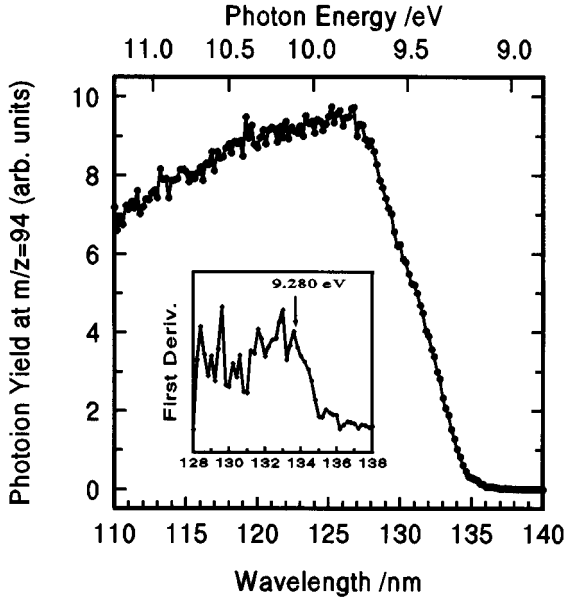

FIG. 3. Photoionization efficiency spectrum of HSC_2H_4SH ($m/z=94$) at a nominal resolution of 0.2 nm and with 0.1 nm steps. The concentration of HSC_2H_4SH in He was 0.2%. The first derivative of the PIE spectrum near the onset region is shown in the inset. The arrow indicates the ionization energy of HSC_2H_4SH.

As in the case of C_2H_5SH, the threshold of photoionization of 2-C_3H_7SH was determined from the maximum of the first derivative of the PIE spectrum, found at (135.6±0.1) nm, as indicated by the arrow in the inset of Fig. 2. This threshold corresponds to an ionization energy of (9.143 ±0.007) eV, in agreement with the value of 9.14 eV measured in a He I photoelectron spectrum.[31]

C. PIE spectrum and IE of HSC_2H_4SH

The PIE spectrum of HSC_2H_4SH shows a more gradually rising onset than those of C_2H_5SH and 2-C_3H_7SH, as depicted in Fig. 3. In contrast to the latter two cases, the first derivative of the PIE spectrum of HSC_2H_4SH near the onset region $\lambda=(128–138)$ nm consists of several maxima as shown in the inset of Fig. 3. The first three features from the right congest to one broad band that we are unable to resolve in terms of either autoionization structure or vibrational progressions of the $HSC_2H_4SH^+$ ion.

In recent *ab initio* calculations, Zhao *et al.*[32] predicted rotational isomers with varied conformations besides the most stable isomer of HSC_2H_4SH that possesses C_{2h} symmetry. The three features in the first derivative curve might involve transitions of rotational isomers of the neutral molecule to their ionic ground states or from the ground state of the neutral molecule to rotational isomers of the ion. We identify the first feature as the threshold for ionization from the ground state of the neutral molecule to the ground state of the ion. The corresponding ionization energy of (9.280 ±0.014) eV is the first such value reported for HSC_2H_4SH.

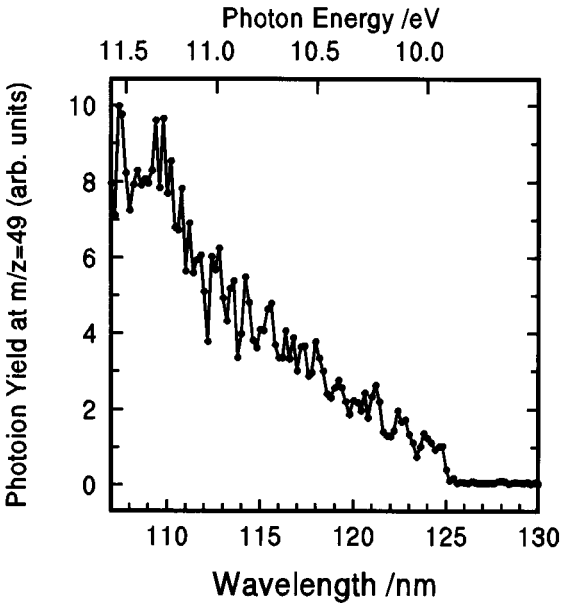

FIG. 4. Photoionization efficiency spectrum of HSO ($m/z=49$) generated from the O+2-C_3H_7SH reaction over the wavelength range (107–130) nm at a nominal resolution of 0.4 nm (slit width 0.2 mm) and with 0.2 nm steps.

D. PIE spectrum and IE of HSO

In order to verify the generation and detection of HSO radicals, the radicals were produced through reactions of atomic oxygen with three organothiol compounds, C_2H_5SH, 2-C_3H_7SH, and HSC_2H_4SH. In Fig. 4 the PIE spectrum of ions at $m/z=49$ (HSO^+) is shown, recorded from the O+2-C_3H_7SH reaction. The spectrum was obtained at 0.2 nm steps with slit width of 0.2 mm in the spectral range $\lambda=(107-130)$ nm. A background ion yield spectrum for $m/z=49$ was also recorded under the same flow conditions except that the microwave discharge to produce O atoms was turned off. There was no structure observed in the background spectrum for wavelengths greater than 107 nm, it only contained small and regular noise. Thus the PIE spectrum displayed in Fig. 4 represents an interference-free spectrum of HSO produced from the O+2-C_3H_7SH reaction. The PIE spectrum is characterized by a step onset at 125 nm and by an increase of the ion yield from the onset up to a plateau at about 110 nm.

PIE spectra of ions at $m/z=49$ generated with an alternative reactant, C_2H_5SH, are depicted in Fig. 5. The upper curve of the ion yield spectrum in Fig. 5(a) was recorded with the microwave discharge on, whereas the lower curve was measured with the microwave discharge off, representing the background signals. In contrast to the case of 2-C_3H_7SH as a reactant, large background signals from the C_2H_5SH reactant appear at 112.5 nm and continue to increase to 107 nm. This background problem is further discussed in the next section. The difference between the two curves in Fig. 5(a) is plotted in Fig. 5(b), which is the PIE spectrum of the HSO radical. Because signals from the reaction product HSO are less than 10% of the total ion counts at

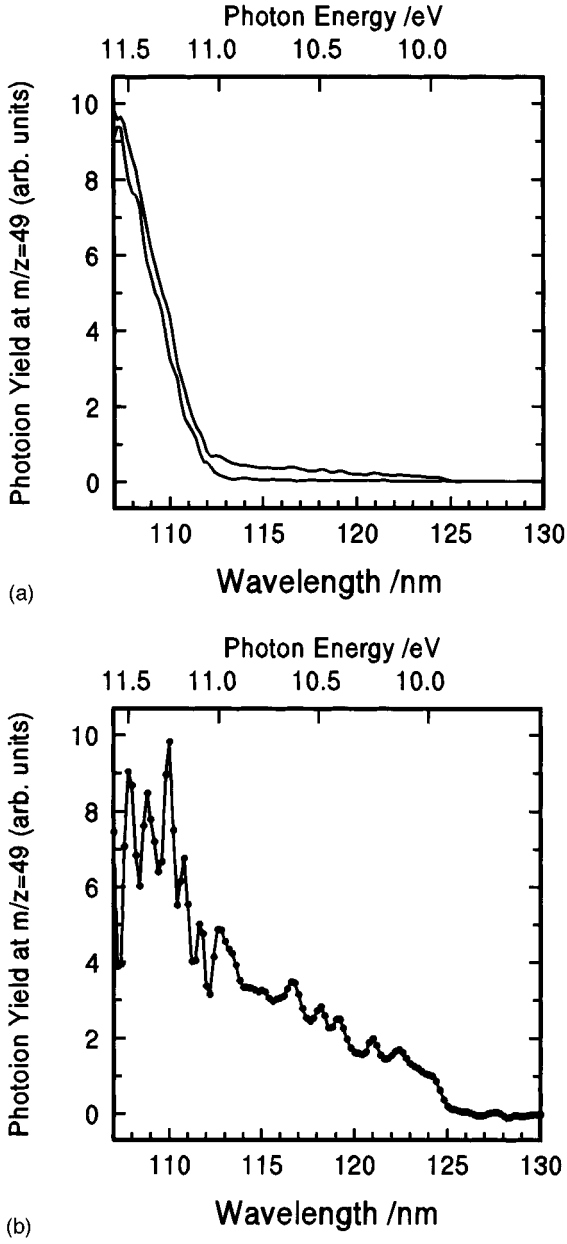

FIG. 5. (a) Photoionization efficiency spectra of ions at $m/z=49$ in the case of C_2H_5SH as reactant to produce HSO. Upper curve: microwave discharge on for generation of O atoms; lower curve: microwave discharge off. Slit width 0.2 mm and scan step 0.2 nm. (b) Plot of the difference between the two curves in (a), enlarged by a factor of 10.

107 nm, the statistical error of the spectrum is large in the wavelength range (107–110) nm. However, the envelope of the curve in Fig. 5(b) is identical to that of Fig. 4. There also occurs a step onset at 125 nm.

We also measured the PIE spectrum of ions at $m/z=49$ from the HSC_2H_4SH reactant. The ion yield in this case was about a factor of 10 smaller than in the case of C_2H_5SH. As in the latter case, large background signals were observed at smaller wavelengths when the microwave discharge was off, but the background appeared at 115.4 nm compared to 112.5 nm in the case of C_2H_5SH. We estimate the ion counts at $m/z=49$ arising from HSO to be about 5%

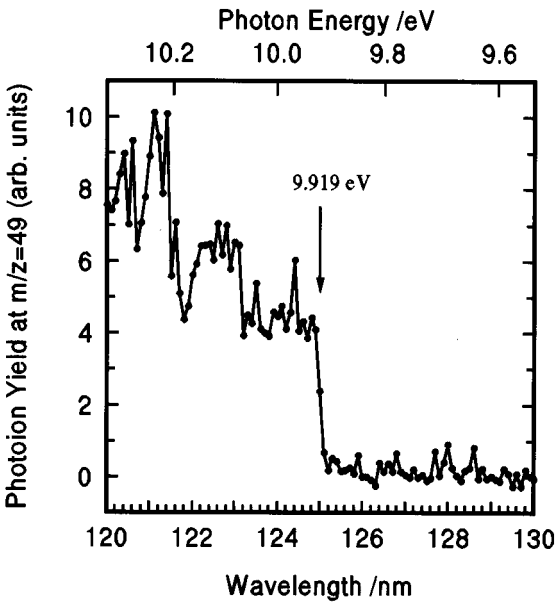

FIG. 6. Photoionization threshold region of HSO over the wavelength range $\lambda=(120-130)$ nm at a nominal resolution of 0.2 nm and with 0.1 nm steps. HSO was generated from the O+2-C_3H_7SH reaction. The arrow indicates the ionization energy of HSO.

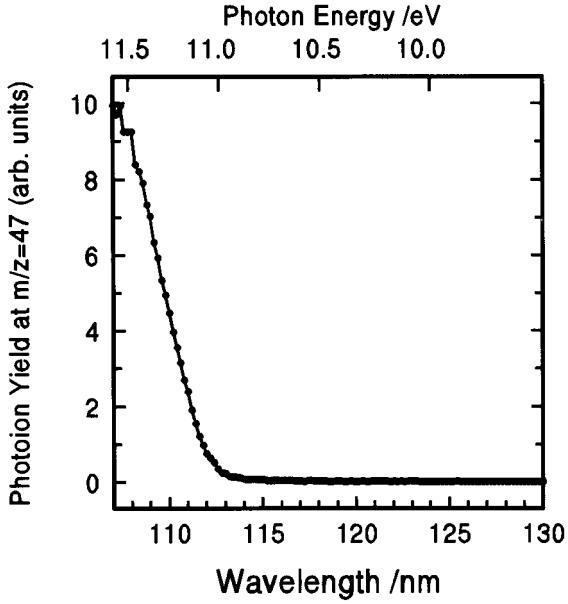

FIG. 7. Photoionization efficiency spectrum of ions at $m/z=47$ from C_2H_5SH. This spectrum is attributed to CH_2SH^+ formed through $CH_3CH_2SH+h\nu\rightarrow CH_3+CH_2SH^++e$.

of the total ion counts at around 110 nm. The resultant PIE spectrum of HSO after subtracting the background signal is therefore of poor quality. However, the overall envelope of the PIE spectrum is quite similar to those shown in Figs. 4 and 5(b) and also a conspicuous step onset occurs at 125 nm.

In order to improve the determination of the ionization energy of HSO, detailed examinations near the threshold region were performed for all three reactions. Figure 6 displays the threshold region of HSO from the O+2-C_3H_7SH reaction over the wavelength range $\lambda=(120-130)$ nm. The spectrum was recorded at a nominal resolution of 0.2 nm (with a slit width of 0.1 mm) and with 0.1 nm steps. The threshold is derived from the distinct step shown at the onset either from the first derivative or from the midrise point of the onset. A threshold of (125.0 ± 0.2) nm was obtained, which corresponds to an ionization energy of (9.919 ± 0.014) eV. Similarly, the ionization energy of HSO was also determined from measurements in the threshold region from the O+C_2H_5SH and O+HSC_2H_4SH reactions. Table II lists all the determinations of the ionization energy of HSO. Taking a simple average, we find the ionization energy of HSO to be (9.918 ± 0.016) eV.

TABLE II. Ionization energies of HSO produced from different reactions.

Reaction	IE/eV
O+C_2H_5SH	9.907 ± 0.014[a]
O+2-C_3H_7SH	9.919 ± 0.014[a]
O+HSC_2H_4SH	9.927 ± 0.014[a]
Average	9.918 ± 0.016[b]

[a]Uncertainty derived from instrumental resolution.
[b]Uncertainty limits represent 2σ.

Beginning from the threshold, three steplike features appear in Fig. 6, which are attributed to a Franck–Condon vibrational progression of HSO^+. Their separation corresponds to a vibrational frequency of (1150 ± 160) cm^{-1}.

E. Appearance energy (AE) of CH_2SH^+

In the background experiments with the microwave discharge off, we detected strong signals at $m/z=49$ starting at 112.5 nm for the system $O_2+C_2H_5SH$ in He, as illustrated in the lower curve of Fig. 5(a). As there were no O atoms present in the flow tube, no HSO radicals were produced and the observed signal therefore arises from some other species. We also monitored the ions at $m/z=47$ under the same flow conditions. At the photoionization wavelength of 110 nm, the ratio of the ion counts recorded at $m/z=49$ and at $m/z=47$ is about 4.5%, which is consistent with the isotope ratio $^{34}S/^{32}S$ in natural abundance. Hence the ions at $m/z=47$ and $m/z=49$ may be $CH_2{}^{32}SH^+$ and $CH_2{}^{34}SH^+$, respectively.

The PIE spectrum of ions at $m/z=47$ from C_2H_5SH is shown in Fig. 7. CH_2SH^+ is generated by fragmentation due to photoionization of CH_3CH_2SH,

$$CH_3CH_2SH+h\nu\rightarrow CH_3+CH_2SH^++e,$$

$$\mathrm{AE}=(11.02\pm0.04)\ \mathrm{eV}. \tag{5}$$

The curve for $m/z=47$ in Fig. 7 is identical to the lower curve for $m/z=49$ in Fig. 5(a), indicating that those signals arise from isotopomers. If we extrapolate the linear portion near 111 nm in Fig. 7, the line will intersect with the background level at (112.5 ± 0.4) nm. This value corresponds to an appearance energy of (11.02 ± 0.04) eV for CH_2SH^+ from CH_3CH_2SH.

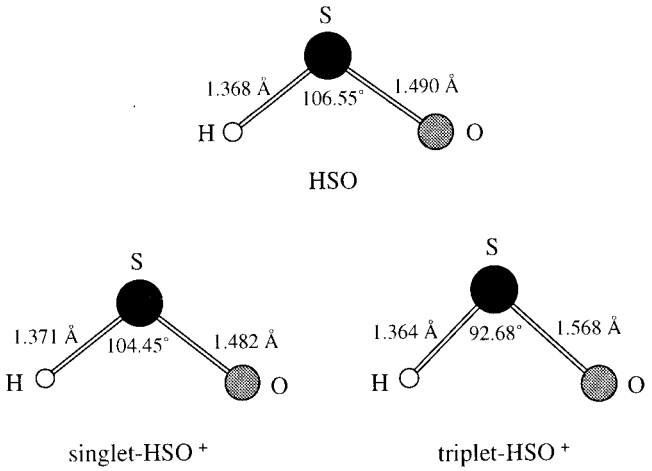

FIG. 8. Optimized structures at MP2(full)/6-31(d) level of HSO, singlet HSO^+, and triplet HSO^+.

In the case of HSC_2H_4SH, we also monitored ions at $m/z=47$ and $m/z=49$ when the microwave discharge was off. In analogy to the discussion above, we conclude that the observed signals arise from $CH_2{}^{32}SH^+$ and $CH_2{}^{34}SH^+$, respectively, and that these ions are formed by photoionization fragmentation of $HSCH_2CH_2SH$,

$$HSCH_2CH_2SH+h\nu\rightarrow CH_2SH+CH_2SH^++e,$$

$$\mathrm{AE}=(10.74\pm0.04)\ \mathrm{eV}. \qquad (6)$$

In the case of 2-C_3H_7SH, as the molecular topology $CH_3CH(SH)CH_3$ contains no CH_2SH moiety, CH_2SH^+ cannot be generated according to a mechanism of photoionization fragmentation similar to reactions (5) and (6). Thus the ions at $m/z=49$ obtained from the reaction system O+2-C_3H_7SH are entirely attributed to HSO^+, free of interference from $CH_2{}^{34}SH^+$. For this reason, the O+2-C_3H_7SH reaction is the most reliable source for HSO in the present experiments.

F. Theoretical results for the IE of HSO

The optimized structures of HSO, singlet HSO^+, and triplet HSO^+ at the MP2(full)/6-31(d) level are depicted in Fig. 8. The structure of singlet HSO^+ is similar to that of neutral HSO. The structure of triplet HSO^+, in contrast, is quite different from that of neutral HSO: the S–O bond in triplet HSO^+ is ≈0.8 Å longer and the bond angle is ≈13° smaller than in neutral HSO.

Table III lists the calculated values of E_{G2}, $E_{G2'}$, IE, and $IE_{vertical}$ of HSO and its cations. For ionization to singlet HSO^+, the calculated values of IE and $IE_{vertical}$ are 9.897 and 9.925 eV, respectively. The calculated values of IE and $IE_{vertical}$ for ionization to triplet HSO^+, are 11.204 and 12.878 eV, respectively. Those values differ by 1.674 eV, whereas for singlet HSO^+ the difference is 0.028 eV. This trend correlates with the structural variations between HSO and its singlet and triplet cations. According to the calculations, the ionization of HSO near the threshold region is more likely to form the singlet ion; the calculated IE of 9.897 eV agrees well with the experimental value of 9.918 eV. As the structure of singlet HSO^+ resembles that of neutral HSO, and as the calculated IE and $IE_{vertical}$ differ by only 0.028 eV, a distinctly sharp onset in the PIE spectrum is expected near the ionization threshold, consistent with our experimental observation. Close inspection of the PIE spectra in Figs. 4 and 5(b) reveals that a discontinuity occurs at ≈(111.2±0.4) nm, corresponding to an energy of (11.15±0.04) eV. According to the calculation, this may indicate an onset to triplet HSO^+.

TABLE III. Calculated E_{G2}, $E_{G2'}$, IE, and $IE_{vertical}$ of HSO and its cations.

	E_{G2} /hartree	$E_{G2'}$ /hartree	IE /eV	$IE_{vertical}$ /eV
HSO	−473.423 673			
Singlet-HSO^+	−473.059 957	−473.058 946	9.897	9.925
Triplet-HSO^+	−473.011 936	−472.950 416	11.204	12.878

TABLE IV. Scaled vibrational frequencies (cm^{-1}) of HSO, singlet-HSO^+, and triplet-HSO^+ calculated at the HF/6-31(d) level.

	ν_1	ν_2	ν_3
HSO	2543	1061	751
Singlet-HSO^+	2518	1104	1285
Triplet-HSO^+	2528	917	890

The vibrational frequency of the bending mode of neutral HSO from the scaled calculation at the HF/6-31(d) level is 1061 cm^{-1}, see Table IV, in satisfactory agreement with the experimental value of 1063 cm^{-1} derived from a chemiluminescence spectrum.[7] The calculated vibrational frequency of the bending mode for singlet HSO^+ is 1104 cm^{-1}, close to the observed vibrational frequency of (1150±160) cm^{-1}. Therefore we tentatively assign this vibrational frequency to the ν_2 mode of singlet HSO^+.

G. Heat of formation of HSO^+

The heat of formation of HSO^+ can be derived from the heat of formation of HSO and IE of HSO. The heat of formation of HSO has been a matter of controversy over the last years. Experimental values vary between $\Delta_f H^\circ_{298}(\mathrm{HSO})\leqslant 14.9$ kcal mol^{-1} and $\Delta_f H^\circ_0(\mathrm{HSO})=-(0.9\pm0.7)$ kcal mol^{-1},[7,33–35] and theoretically deduced values range from $\Delta_f H^\circ_0(\mathrm{HSO})=(0.3\pm3.0)$ kcal mol^{-1} to $\Delta_f H^\circ_{298}(\mathrm{HSO})\leqslant-(6.1\pm1.3)$ kcal mol^{-1}.[36–42] A recent compilation recommends $\Delta_f H^\circ_{298}(\mathrm{HSO})=-(1\pm5)$ kcal mol^{-1},[43] close to the latest experimental value reported.[35] Taking this recommended value for $\Delta_f H^\circ_{298}(\mathrm{HSO})$ and the value from this work for IE of HSO, the heat of formation of HSO^+ is calculated to be $\Delta_f H^\circ_{298}(HSO^+)=(228\pm5)$ kcal mol^{-1}.

IV. CONCLUSIONS

The PIE spectrum of HSO was measured for the first time with a discharge-flow system coupled to a photoionization mass spectrometer that employs synchrotron radiation as

the ionizing source. HSO radicals were produced from reactions of O atoms with various organothiol compounds, C_2H_5SH, 2-C_3H_7SH, or HSC_2H_4SH, in the flow tube. Among those, the O+2-C_3H_7SH reaction was found to be the best suited source for generation of HSO radicals as there was no interference from fragments arising from the photoionization. The PIE spectrum of HSO displays a distinctly sharp onset. The threshold for ionization of the ground state of HSO to singlet HSO^+ was determined to be (9.918 $\pm$0.016) eV. This result agrees satisfactorily with theoretical calculations using the G2 method. The onset for ionization of the ground state of HSO to triplet HSO^+ may occur at about (11.15$\pm$0.04) eV. One vibrational frequency of HSO^+ was found to be (1150$\pm$160) cm^{-1}, which we tentatively assign to the ν_2 bending mode. The heat of formation of HSO^+ is calculated to be $\Delta_f H^\circ_{298}(HSO^+)=(228\pm5)$ kcal mol^{-1}.

ACKNOWLEDGMENTS

The support of the Synchrotron Radiation Research Center of Taiwan and the National Science Council of the Republic of China (Contract No. NSC 86-2613-M-213-019-L1) is gratefully acknowledged. We thank the National Center for High-performance Computation for computing time.

[1] G. S. Tyndall and A. R. Ravishankara, Int. J. Chem. Kinet. **23**, 483 (1991).
[2] M. T. Leu and R. H. Smith, J. Phys. Chem. **86**, 73 (1982).
[3] N. D. Sze and M. K. W. Ko, Atmos. Environ. **4**, 1223 (1980).
[4] R. A. Cox and F. J. Sandalls, Atmos. Environ. **8**, 1269 (1974).
[5] G. Schönle, M. M. Rahman, and R. N. Schindler, Ber. Bunsenges. Phys. Chem. **91**, 66 (1987).
[6] R. N. Schindler and Th. Benter, Ber. Bunsenges. Phys. Chem. **92**, 588 (1988).
[7] U. Schurath, M. Weber, and K. H. Becker, J. Chem. Phys. **67**, 110 (1977).
[8] D. J. W. Kendall, J. J. A. O'Brien, J. J. Sloan, and R. G. MacDonald, Chem. Phys. Lett. **110**, 183 (1984).
[9] M. T. Leu and R. H. Smith, J. Phys. Chem. **85**, 2570 (1981).
[10] V. P. Bulatov, M. Z. Kozliner, and O. M. Sarkisov, Khim. Fiz. **3**, 988 (1984).
[11] M. Kawasaki, K. Kasatani, and H. Sato, Chem. Phys. Lett. **75**, 128 (1980).
[12] I. R. Slagle, R. E. Graham, and D. Gutman, Int. J. Chem. Kinet. **8**, 451 (1976).
[13] M. Kakimoto, S. Saito, and E. Hirota, J. Mol. Spectrosc. **80**, 334 (1980).
[14] M. Satoh, N. Ohashi, and S. Matsuoka, Bull. Chem. Soc. Jpn. **56**, 2545 (1983).
[15] C. R. Webster, P. J. Brucat, and R. N. Zare, J. Mol. Spectrosc. **92**, 184 (1982).
[16] N. Ohashi, S. Saito, T. Suzuki, and E. Hirota, J. Mol. Spectrosc. **127**, 481 (1988).
[17] Y. Takehisa and N. Ohashi, J. Mol. Spectrosc. **130**, 221 (1988).
[18] T. J. Sears and A. R. W. Mckellar, Mol. Phys. **49**, 25 (1983).
[19] Y. Endo, S. Saito, and E. Hirota, J. Chem. Phys. **75**, 4379 (1981).
[20] E. R. Lovejoy, N. S. Wang, and C. J. Howard, J. Phys. Chem. **91**, 5749 (1987).
[21] V. P. Bulatov, M. Z. Kosliner, and O. M. Sarkisov, Khim. Fiz. **3**, 1300 (1984).
[22] V. P. Bulatov, M. Z. Kosliner, and O. M. Sarkisov, Khim. Fiz. **4**, 1353 (1985).
[23] V. P. Bulatov, O. M. Sarkisov, M. Z. Kosliner, and V. G. Egorov, Khim. Fiz. **5**, 1031 (1986).
[24] (a) B.-M. Cheng and W.-C. Hung, J. Phys. Chem. **100**, 10210 (1996); (b) W.-C. Hung, M.-Y. Shen, Y.-P. Lee, N.-S. Wang, and B.-M. Cheng, J. Chem. Phys. **105**, 7402 (1996).
[25] I. R. Slagle, F. Balocchl, and D. Gutman, J. Phys. Chem. **82**, 1333 (1978).
[26] P.-C. Tseng *et al.*, Rev. Sci. Instrum. **66**, 1815 (1995).
[27] B.-M. Cheng, W.-J. Lo, and W.-C. Hung, Chem. Phys. Lett. **236**, 355 (1995).
[28] L. A. Curtiss, K. Raghavachari, G. W. Trucks, and J. A. Pople, J. Chem. Phys. **94**, 7221 (1991).
[29] GAUSSIAN 94 (Revision D.2), M. J. Frisch, G. W. Trucks, H. B. Schlegel, P. M. W. Gill, B. G. Johnson, M. A. Robb, J. R. Cheeseman, T. A. Keith, G. A. Petersson, J. A. Montgomery, K. Raghavachari, M. A. Al-Laham, V. G. Zakrzewski, J. V. Ortiz, J. B. Foresman, J. Cisolowski, B. B. Stefanov, A. Nanayakkara, M. Challacombe, C. Y. Peng, P. Y. Ayala, W. Chen, M. W. Wong, J. L. Andres, E. S. Replogle, R. Gomperts, R. L. Martin, D. J. Fox, J. S. Binkley, D. J. Defrees, J. Baker, J. J. P. Stewart, M. Head-Gordon, C. Gonzalez, and J. A. Pople, Gaussian, Inc., Pittsburgh, PA, 1995.
[30] K. Watanabe, T. Nakayama, and J. Mottl, J. Quant. Spectrosc. Radiat. Transf. **2**, 369 (1962).
[31] H. Ogata, H. Onizuka, Y. Nihei, and H. Kamada, Bull. Chem. Soc. Jpn. **46**, 3036 (1973).
[32] H.-Q. Zhao, Y.-S. Cheung, C.-X. Liao, C. Y. Ng, W.-K. Li, and S.-W. Chiu, J. Chem. Phys. **104**, 130 (1996).
[33] I. R. Slagle, F. Baiocchi, and D. Gutman, J. Phys. Chem. **82**, 1333 (1978).
[34] F. E. Davidson, A. R. Clemo, D. L. Duncan, R. J. Browett, J. H. Hobson, and R. Grice, Mol. Phys. **46**, 33 (1985).
[35] N. Balucani, P. Casavecchia, D. Stranges, and G. G. Volpi, Chem. Phys. Lett. **211**, 469 (1993).
[36] B. T. Luke and A. D. McLean, J. Phys. Chem. **89**, 4592 (1985).
[37] S. S. Xantheas and T. H. Dunning, Jr., J. Phys. Chem. **97**, 18 (1993).
[38] J. Espinosa-Garcia and J. C. Corchado, Chem. Phys. Lett. **218**, 128 (1994).
[39] M. Esseffar, O. Mó, and Yáñez, J. Chem. Phys. **101**, 2175 (1994).
[40] C. Wilson and D. M. Hirst, J. Chem. Soc. Faraday Trans. **90**, 3051 (1994).
[41] A. Goumri, D. Laakso, J.-D. R. Rocha, C. E. Smith, and P. Marshall, J. Chem. Phys. **102**, 161 (1995).
[42] S. S. Xantheas and T. H. Dunning, Jr., J. Phys. Chem. **97**, 6616 (1993).
[43] W. B. DeMore, S. P. Sander, D. M. Golden, R. F. Hampson, M. J. Kurylo, C. J. Howard, A. R. Ravishankara, C. E. Kolb, and M. J. Molina, Evaluation No. 11, JPL Publ. No. 94-26 (1994).